

**Large exchange bias field and its coupling-controlled sign reversal in a van der
Waals heterostructure of CrI₃/MnBi₂Te₄ ferromagnetic
insulator/antiferromagnetic topological insulator**

Zhe Ying^{1, #}, Bo Chen^{1, #}, Chunfeng Li¹, Boyuan Wei¹, Zheng Dai¹, Fengyi Guo¹,
Danfeng Pan^{2, 3}, Haijun Zhang¹, Di Wu¹, Xuefeng Wang², Shuai Zhang^{1, 4*}, Fucong
Fei^{1, 4*} and Fengqi Song^{1, 4*}

¹ National Laboratory of Solid State Microstructures, Collaborative Innovation Center
of Advanced Microstructures, and School of Physics, Nanjing University, Nanjing
210093, China

² National Laboratory of Solid State Microstructures, Collaborative Innovation Center
of Advanced Microstructures, and School of Electronic Science and Engineering,
Nanjing University, Nanjing 210093, China

³ Microfabrication and Integration Technology Center, Nanjing University, Nanjing
210093, China

⁴ Atom Manufacturing Institute, Nanjing 210093, China

[#]Z.Y. and B.C. contributed to the work equally.

^{*}Corresponding author.

Email: S.Z. (szhang@nju.edu.cn), F.F. (feifucong@nju.edu.cn) and F.S.
(songfengqi@nju.edu.cn).

Abstract:

Here we fabricate the van der Waals heterostructure devices with ferromagnetic insulator CrI_3 nanoflakes and few-layers antiferromagnetic topological insulator MnBi_2Te_4 and study the exchange bias behavior. The devices originally exhibit a negative exchange bias effect, which size decays with the increasing temperature and stays unchanged while tuning the back-gate voltage. When the device configuration turns to partially covered by CrI_3 , the exchange bias becomes positive with a very large exchange bias field of over 300 mT. Such sensitive manipulation is interpreted by the competitive onset of the ferromagnetic and antiferromagnetic coupling through the interface of CrI_3 and MnBi_2Te_4 , pointing to tunable interface interactions and controlled quantum anomalous Hall state manipulation.

Introduction

Since the discovery of quantum anomalous Hall (QAH) effect in magnetically doped topological insulator (TI), researchers have devoted many efforts to explore new physics with the help of this novel state[1,2]. To avoid random magnetic dopants, MnBi_2Te_4 was theoretically proposed as an intrinsic antiferromagnetic (AFM) TI [3-7]. As a layered van der Waals (vdW) material, each layer of MnBi_2Te_4 is a septuple-layer (SL) and two neighboring layers are stacked weakly by vdW forces (inset of Fig. 1b). Within each SL, the Mn^{2+} moments are aligned ferromagnetically along the [0001] direction, while adjacent SLs are antiferromagnetically coupled. Subsequent experimental works have verified this prediction with the realization of zero-field QAH state [8], high-field Chern insulator state [9-12] and axion insulator state [13] in exfoliated MnBi_2Te_4 thin flakes.

However, the magnetic moments on the top surface of MnBi_2Te_4 were suspected to be complex and different from ideal situation [2,14,15], often resulting in even obliterated magnetic topological gap and, hence, the absence of QAH state. Therefore, improving the reproducibility and quality of the zero-field QAH state through surface/interface engineering of MnBi_2Te_4 is a central task of the community to achieve a practical QAH device. According to the theoretical prediction, magnetic proximity the MnBi_2Te_4 to a magnetic insulator, such as CrI_3 , would facilitate the QAH state formation, which results from the large exchange interaction at the interface between MnBi_2Te_4 and CrI_3 [16]. In addition, given that both MnBi_2Te_4 and CrI_3 holds a sizable magnetic anisotropy with an out-of-plane easy axis [3,17-19], the heterostructure

device of MnBi_2Te_4 and CrI_3 is believed to be a very promising system that deserve investigation.

Here we fabricate the FM/AFM heterostructure devices of $\text{CrI}_3/\text{MnBi}_2\text{Te}_4$ by dry transfer technique [20-22] and measure their electrical transport upon magnetic fields. Although zero-field QAH effect is absent, lateral shift of hysteresis loops, i.e. exchange bias effect, are successfully observed. A large exchange bias field is revealed, and it reverses its sign and reaches over 0.3 Tesla while changing the CrI_3 covering configuration on the MnBi_2Te_4 layer. Our work demonstrates the magnetic coupling physics through the interface of $\text{CrI}_3/\text{MnBi}_2\text{Te}_4$ and potentially paves the way towards controlled QAH states.

Results

Few-SLs MnBi_2Te_4 and CrI_3 nanoflakes were mechanically exfoliated from bulk crystals. When the MnBi_2Te_4 field-effect transistor (FET) device is fabricated, we stack the CrI_3 nanoflake on top of the MnBi_2Te_4 device to form the $\text{CrI}_3/\text{MnBi}_2\text{Te}_4$ heterostructure (inset of Fig. 1(b)). The thickness of CrI_3 nanoflakes is about 20 nm in this study, which are thin enough that we can stack it above MnBi_2Te_4 to form an interface with satisfied quality due to its flexibility, even though there are pre-patterned electrodes. Meanwhile, the ~ 20 nm thick CrI_3 nanoflake can suppress thermal fluctuations and holds a more stable magnetic anisotropy. More details about device fabrications are contained in Methods. Figure 1(a) is the schematic configuration of a $\text{CrI}_3/\text{MnBi}_2\text{Te}_4$ heterostructure device. The graphite and hexagonal boron nitride (h-BN)

flakes are used to protect the CrI_3 and MnBi_2Te_4 sample from degradation [17].

An optical image of a $\text{CrI}_3/(5\text{-SLs})\text{MnBi}_2\text{Te}_4$ device (labeled as D1 hereafter) before h-BN and graphite protective layer capping is shown in the inset of Fig. 1(b). Figure 1(b) is the back-gate (V_{bg}) dependent longitudinal resistance (R_{xx}) of D1 at zero magnetic field, which suggests that the carrier in this range is hole type. To study the exchange bias effect, we follow the traditional measurement methodology of field cooling treatment [23-25]. Given that the Curie temperature (T_C) of bulk CrI_3 and Néel temperature (T_N) of MnBi_2Te_4 crystals are ~ 61 K and ~ 24 K, respectively, we increase the temperature (T) to 80 K, and then apply a magnetic field (cooling field, $\mu_0 H_{\text{cf}}$) that perpendicular to the sample plane for polarization. Figure 1(c) is the temperature dependent R_{xx} during field-cooling processes. As reported previously, the dip or hump feature around 21 K in $R_{\text{xx}} - T$ curves indicate the Néel temperature of MnBi_2Te_4 thin films [8,26]. When the sample is cooled to the measurement temperature, we measure the magnetic-field dependent Hall resistance (R_{yx}). The magnetic field is perpendicular to the sample plane as well.

Negative exchange bias effect in fully covered $\text{CrI}_3/\text{MnBi}_2\text{Te}_4$ devices.

As a typical ferromagnetic/antiferromagnetic (FM/AFM) bilayer heterostructure, the $\text{CrI}_3/\text{MnBi}_2\text{Te}_4$ devices can be an ideal host for the exchange bias effect [27-29]. A lateral shift of hysteresis loop is the key feature of exchange bias effect, and many commercial applications benefit from this effect [29,30]. The first (1st) curve in Fig. 1(d) is the typical R_{yx} loop measured after field cooled at $\mu_0 H_{\text{cf}} = -0.5$ T, from which a remarkable lateral shift along the horizontal axis towards positive field can be found.

Since the direction of lateral shift is opposite to the direction of cooling-field, therefore, it is negative exchange bias effect by definition [23,24,28]. The training effect of exchange bias is also shown in Fig. 1(d), i.e., as we repeat the R_{yx} loop measurement successively, the exchange bias effect is going to disappear gradually [29,31]. In another $\text{CrI}_3/(7\text{-SLs})\text{MnBi}_2\text{Te}_4$ device (labeled as D2 hereafter) shown in Fig. S3, we also observed negative exchange bias effect. Furthermore, the Chern insulator state can be observed in D2 as well (Fig. S1). The training effect of D2 is shown in Fig. S3, where exchange bias decreases more slowly than D1 here. Given the training effect, all R_{yx} loops in the rest of this paper are the first loop measured after field-cooling treatment.

To study whether the exchange-bias field ($\mu_0 H_{eb} = (\text{right coercive field} + \text{left coercive field})/2$), which is a quantitative description of the lateral shift of hysteresis loop [28,29], would be affected by the carrier density or not, we measure the exchange bias effect under different V_{bg} (Fig. 2a). In the V_{bg} ranges that we investigate, $\mu_0 H_{eb}$ only shows negligible fluctuations. The same V_{bg} independent behavior of $\mu_0 H_{eb}$ observed in D2 is shown in Fig. S4. When it comes to exchange bias effect, it is also essential to investigate the influences of cooling field [23,30]. Figure 2(b) is exchange bias effect of D1 measured after field cooled at different cooling fields. As the cooling field is positive, the resulted R_{yx} loop shift toward negative field all the time and the magnitude of lateral shift are quite stable, no matter the magnitude of cooling field.

To explore the blocking temperature, i.e., the temperature above which the exchange bias effect disappears [28], we carry out the measurement by varying

temperatures. Figure 2(c) (Fig S4) shows the results of D1 (D2). The temperature dependent $\mu_0 H_{eb}$ of D1 and D2 are extracted and plotted in Fig. 2(d). The blocking temperature in D1 is 9 K and it is higher than ~ 5 K in D2, which might be an evidence that D1 has a better interfacial quality than D2 (note that the quality of heterostructures fabricated by dry transfer technique usually vary from sample to sample). And both blocking temperatures are less than the Néel temperature of MnBi_2Te_4 thin flake (~ 21 K). The coercive field ($\mu_0 H_c$) is defined as (right coercive field – left coercive field)/2. Figure 2(e) is the corresponding temperature dependent $\mu_0 H_c$. Despite that there are relevant differences in $\mu_0 H_c$ between D1 and D2, the observed $\mu_0 H_{eb}$ is at the same level (~ 150 mT) at low temperature (~ 2 K).

Positive exchange bias effect in partially covered $\text{CrI}_3/\text{MnBi}_2\text{Te}_4$ devices.

To achieve further manipulation, we fabricate the partially covered $\text{CrI}_3/\text{MnBi}_2\text{Te}_4$ heterostructure devices, where the MnBi_2Te_4 is partially covered by a CrI_3 nanoflake, as illustrated in Fig. 3(a). Particularly, the R_{yx} is measured on bare MnBi_2Te_4 region not covered by CrI_3 layer. Figure 3(b) is an optical image of a partially covered $\text{CrI}_3/\text{MnBi}_2\text{Te}_4$ heterostructure device (labeled as D4 hereafter), and the thickness of MnBi_2Te_4 in D4 is 7 SLs. Figures 3(c, d) are temperature dependent exchange bias effect observed in D4 that field cooled at 0.1 T and -0.1 T, respectively. As the lateral shift direction of R_{yx} loop is consistent with the direction of cooling field, it is positive exchange bias effect [23,24] in D4, being different from the preceding fully covered devices D1 and D2. The extracted $\mu_0 H_{eb}$ versus temperature are plotted in Fig. 3(e), from which a blocking temperature of ~ 18 K can be found, and it is close to the Néel

temperature of MnBi_2Te_4 thin flakes. Remarkably, the $\mu_0 H_{\text{eb}}$ could be greater than 300 mT at ~ 10 K. Temperature dependent coercive fields are summarized in Fig. 3(f) as well. Obviously, both the $\mu_0 H_{\text{eb}}$ and $\mu_0 H_{\text{c}}$ are enhanced in the partially covered $\text{CrI}_3/\text{MnBi}_2\text{Te}_4$ device.

Discussions

As the positive exchange bias phenomenon is detected in bare MnBi_2Te_4 that beyond the $\text{CrI}_3/\text{MnBi}_2\text{Te}_4$ heterostructure region, we first speculate that these observations are induced by stray fields [32] of CrI_3 layer. The stray fields of CrI_3 layer experienced by MnBi_2Te_4 outside the heterostructure region has opposite direction to that experienced by MnBi_2Te_4 beneath the CrI_3 layer. Intuitively, this seems to explain why bare MnBi_2Te_4 region in D4 can be biased oppositely to the MnBi_2Te_4 beneath CrI_3 as in D1 and D2. However, this explanation is invalid and denied by our control experiment in another partially covered $\text{CrI}_3/\text{MnBi}_2\text{Te}_4$ device (labeled as D3 hereafter), where the R_{yx} of bare MnBi_2Te_4 and CrI_3 -covered MnBi_2Te_4 are detected simultaneously. The positive exchange bias effect is observed in both regions. Moreover, two regions have identical coercive field (Fig. S6). This makes us believe that MnBi_2Te_4 is exchange biased consistently not separately. In addition, given the smaller coercive field of CrI_3 compared with MnBi_2Te_4 , the stray field of CrI_3 is unlikely to be able to bias the hysteresis loop of MnBi_2Te_4 as well.

Exchange bias effect originates from the unidirectional anisotropy induced by exchange interaction between FM and AFM layer at the heterostructure interface

[24,28]. Generally, in FM/AFM bilayer heterostructures, the negative (positive) exchange bias effect is a result of FM (AFM) interfacial coupling, i.e., magnetic moments belong to different materials favor FM (AFM) alignment at the interface [23,28,33]. Based on this consideration, we would conclude that the interfacial coupling in the fully (partially) covered CrI₃/MnBi₂Te₄ heterostructures is FM (AFM) type (Fig. 4(a)). During the field cooling process with a small $\mu_0 H_{\text{cf}}$, the FM ordering of CrI₃ is formed as the temperature is lower than ~ 61 K. Since $\mu_0 H_{\text{cf}}$ is small, it is the exchange coupling energy between FM and AFM layer rather than the Zeeman energy induced by $\mu_0 H_{\text{cf}}$ that dominates [23]. Therefore, when temperature is lower than ~ 21 K, due to different interfacial coupling type, MnBi₂Te₄ would be ordered differently in fully- and partially-covered configuration. Since the behavior of exchange bias effect is quite sensitive to heterostructure details and sample-dependent [24,34], it is highly possible that the interfacial coupling type would be altered with the varying of interface configuration. The competitive switching between FM and AFM interfacial coupling were observed in oxidized Fe₃GeTe₂ nanoflakes by protonic gate tuning as well [35]. The magnetic force microscopy (MFM) or reflective magnetic circular dichroism (RMCD) imaging would provide further understanding of the observations here, but these experiments are beyond the scope of the present study.

We note that the exchange bias effect reported in this study is revealed in the AFM layer (MnBi₂Te₄ here), which is different from usual situations [23,24,28]. The large exchange bias field observed in CrI₃/MnBi₂Te₄ heterostructure is outstanding compared with several other vdW FM/AFM heterostructures studied in recent years. In Figure

4(b), we summarize the exchange bias field observed in other works for comparison. As these works measure R_{yx} as well, we define a reduced temperature as measurement temperature divided by Curie (or Néel) temperature of the material that contributes R_{yx} signal (Table S1). An alternative definition of the reduced temperature would be measurement temperature divided by blocking temperature as suggested in Ref. 28. Since not all works explored the blocking temperature, our definition is reasonable and informative as well for a qualitative comparison. Obviously, the large exchange bias field observed in $\text{CrI}_3/\text{MnBi}_2\text{Te}_4$ vdW heterostructure is striking.

In summary, we demonstrate the exchange bias effect in the $\text{CrI}_3/\text{MnBi}_2\text{Te}_4$ vdW heterostructure devices. By adjusting the heterostructure configuration, negative and positive exchange bias effect are observed in fully covered and partially covered $\text{CrI}_3/\text{MnBi}_2\text{Te}_4$ devices, respectively. This partially proximity approach for magnetic-engineering would also work in other magnetic vdW heterostructures and deserve further investigations. The large exchange bias field in our experiment confirms the efficient interfacial coupling between CrI_3 and MnBi_2Te_4 . Our work will facilitate the development of antiferromagnetic spintronics [36] and pave the way for potential QAH state manipulation based on antiferromagnetic topological insulators.

Methods:

Device fabrication: MnBi_2Te_4 bulk crystals were grown by flux method as previously reported [4]. High-quality CrI_3 crystals were synthesized by chemical vapor transport

method with the agent of I_2 . Few-layers $MnBi_2Te_4$ and thin flakes of CrI_3 (h-BN, graphite) were mechanically exfoliated onto SiO_2/Si substrate with a SiO_2 thickness of ~ 300 nm and Polydimethylsiloxane (PDMS) substrate, respectively. The electrode pattern was defined by electron beam lithography, then the Au film was evaporated to form electrical contact. After the lift-off processes, we sequentially stacked the pre-exfoliated CrI_3 , h-BN and graphite on top of the $MnBi_2Te_4$. Most of the fabrication processes were carried out in a glove box with H_2O and O_2 contents < 0.1 ppm.

Transport measurements: The electrical transport measurement was conducted in a refrigerator with the base temperature of 1.6 K and 12 T superconducting magnet. The Hall resistance R_{yx} are measured using standard lock-in amplifier technique with an a.c. excitation current of 50 nA at 13 Hz. The applied magnetic field are perpendicular to the sample plane. The R_{yx} data shown in Fig. 3 were antisymmetrized to remove the mixing of Hall resistance and longitudinal resistance induced by the irregular sample geometry [8,30]. The raw data of Fig. 3 is shown in Fig. S5. All the other R_{yx} data shown in the main text and Supporting Information are raw data.

Acknowledgments

We gratefully acknowledge the financial support of the National Key R&D Program of China (No. 2017YFA0303203), the National Natural Science Foundation of China (Grant Nos. 92161201, 12104221, 12025404, 12004174, 11904165, 11904166, 61822403, and 11874203), the Natural Science Foundation of Jiangsu Province (Grant

Nos. BK20200312, BK20200310, and BK20190286), and the Fundamental Research Funds for the Central Universities (Nos. 020414380192).

Conflicts of interest

The authors declare no conflicts of interests.

References

- [1] C.-Z. Chang, J. Zhang, X. Feng, J. Shen, Z. Zhang, M. Guo, K. Li, Y. Ou, P. Wei, L.-L. Wang, Z.-Q. Ji, Y. Feng, S. Ji, X. Chen, J. Jia, X. Dai, Z. Fang, S.-C. Zhang, K. He, Y. Wang, L. Lu, X.-C. Ma, and Q.-K. Xue, *Science* **340**, 167 (2013).
- [2] C.-Z. Chang, C.-X. Liu, and A. H. MacDonald, arXiv:2202.13902.
- [3] M. M. Otrokov, I. I. Klimovskikh, H. Bentmann, D. Estyunin, A. Zeugner, Z. S. Aliev, S. Gaß, A. U. B. Wolter, A. V. Koroleva, A. M. Shikin, M. Blanco-Rey, M. Hoffmann, I. P. Rusinov, A. Y. Vyazovskaya, S. V. Eremeev, Y. M. Koroteev, V. M. Kuznetsov, F. Freyse, J. Sánchez-Barriga, I. R. Amiraslanov, M. B. Babanly, N. T. Mamedov, N. A. Abdullayev, V. N. Zverev, A. Alfonsov, V. Kataev, B. Büchner, E. F. Schwier, S. Kumar, A. Kimura, L. Petaccia, G. Di Santo, R. C. Vidal, S. Schatz, K. Kißner, M. Ünzelmann, C. H. Min, S. Moser, T. R. F. Peixoto, F. Reinert, A. Ernst, P. M. Echenique, A. Isaeva, and E. V. Chulkov, *Nature* **576**, 416 (2019).
- [4] B. Chen, F. Fei, D. Zhang, B. Zhang, W. Liu, S. Zhang, P. Wang, B. Wei, Y. Zhang, Z. Zuo, J. Guo, Q. Liu, Z. Wang, X. Wu, J. Zong, X. Xie, W. Chen, Z. Sun, S. Wang, Y. Zhang, M. Zhang, X. Wang, F. Song, H. Zhang, D. Shen, and B. Wang, *Nature Communications* **10**, 4469 (2019).
- [5] J. Li, Y. Li, S. Du, Z. Wang, B.-L. Gu, S.-C. Zhang, K. He, W. Duan, and Y. Xu, *Science Advances* **5**, eaaw5685 (2019).
- [6] E. D. L. Rienks, S. Wimmer, J. Sánchez-Barriga, O. Caha, P. S. Mandal, J. Růžička, A. Ney, H. Steiner, V. V. Volobuev, H. Groiss, M. Albu, G. Kothleitner, J. Michalička, S. A. Khan, J. Minár, H. Ebert, G. Bauer, F. Freyse, A. Varykhalov, O. Rader, and G. Springholz, *Nature* **576**, 423 (2019).
- [7] M. M. Otrokov, I. P. Rusinov, M. Blanco-Rey, M. Hoffmann, A. Y. Vyazovskaya, S. V. Eremeev, A. Ernst, P. M. Echenique, A. Arnau, and E. V. Chulkov, *Physical Review Letters* **122**, 107202 (2019).
- [8] Y. Deng, Y. Yu, Z. Shi Meng, Z. Guo, Z. Xu, J. Wang, H. Chen Xian, and Y. Zhang, *Science* **367**, 895 (2020).
- [9] J. Ge, Y. Liu, J. Li, H. Li, T. Luo, Y. Wu, Y. Xu, and J. Wang, *National Science Review* **7**, 1280 (2020).
- [10] D. Ovchinnikov, X. Huang, Z. Lin, Z. Fei, J. Cai, T. Song, M. He, Q. Jiang, C. Wang, H. Li, Y. Wang, Y. Wu, D. Xiao, J.-H. Chu, J. Yan, C.-Z. Chang, Y.-T. Cui, and X. Xu, *Nano Letters* **21**, 2544 (2021).
- [11] Z. Ying, S. Zhang, B. Chen, B. Jia, F. Fei, M. Zhang, H. Zhang, X. Wang, and F. Song, *Physical Review B* **105**, 085412 (2022).
- [12] A. Gao, Y.-F. Liu, C. Hu, J.-X. Qiu, C. Tzschaschel, B. Ghosh, S.-C. Ho, D. Bérubé, R. Chen, H. Sun, Z. Zhang, X.-Y. Zhang, Y.-X. Wang, N. Wang, Z. Huang, C. Felser, A. Agarwal, T. Ding, H.-J. Tien, A. Akey, J. Gardener, B. Singh, K. Watanabe, T. Taniguchi, K. S. Burch, D. C. Bell, B. B. Zhou, W. Gao, H.-Z. Lu, A. Bansil, H. Lin, T.-R. Chang, L. Fu, Q. Ma, N. Ni, and S.-Y. Xu, *Nature* **595**, 521 (2021).
- [13] C. Liu, Y. Wang, H. Li, Y. Wu, Y. Li, J. Li, K. He, Y. Xu, J. Zhang, and Y. Wang, *Nature Materials* **19**, 522 (2020).
- [14] Y.-J. Hao, P. Liu, Y. Feng, X.-M. Ma, E. F. Schwier, M. Arita, S. Kumar, C. Hu, R. e. Lu, M. Zeng, Y. Wang, Z. Hao, H.-Y. Sun, K. Zhang, J. Mei, N. Ni, L. Wu, K. Shimada, C. Chen, Q. Liu, and C. Liu, *Physical Review X* **9**, 041038 (2019).
- [15] P. Swatek, Y. Wu, L.-L. Wang, K. Lee, B. Schrunk, J. Yan, and A. Kaminski, *Physical Review B* **101**, 161109 (2020).
- [16] H. Fu, C.-X. Liu, and B. Yan, *Science Advances* **6**, eaaz0948 (2020).

- [17] C. Gong and X. Zhang, *Science* **363**, eaav4450 (2019).
- [18] B. Huang, G. Clark, E. Navarro-Moratalla, D. R. Klein, R. Cheng, K. L. Seyler, D. Zhong, E. Schmidgall, M. A. McGuire, D. H. Cobden, W. Yao, D. Xiao, P. Jarillo-Herrero, and X. Xu, *Nature* **546**, 270 (2017).
- [19] K. F. Mak, J. Shan, and D. C. Ralph, *Nature Reviews Physics* **1**, 646 (2019).
- [20] A. Castellanos-Gomez, M. Buscema, R. Molenaar, V. Singh, L. Janssen, H. S. J. van der Zant, and G. A. Steele, *2D Materials* **1**, 011002 (2014).
- [21] G. Hu, Y. Zhu, J. Xiang, T.-Y. Yang, M. Huang, Z. Wang, Z. Wang, P. Liu, Y. Zhang, C. Feng, D. Hou, W. Zhu, M. Gu, C.-H. Hsu, F.-C. Chuang, Y. Lu, B. Xiang, and Y.-L. Chueh, *ACS Nano* **14**, 12037 (2020).
- [22] H. Dai, H. Cheng, M. Cai, Q. Hao, Y. Xing, H. Chen, X. Chen, X. Wang, and J.-B. Han, *ACS Applied Materials & Interfaces* **13**, 24314 (2021).
- [23] F. Wang, D. Xiao, W. Yuan, J. Jiang, Y.-F. Zhao, L. Zhang, Y. Yao, W. Liu, Z. Zhang, C. Liu, J. Shi, W. Han, M. H. W. Chan, N. Samarth, and C.-Z. Chang, *Nano Letters* **19**, 2945 (2019).
- [24] L. Pan, A. Grutter, P. Zhang, X. Che, T. Nozaki, A. Stern, M. Street, B. Zhang, B. Casas, Q. L. He, E. S. Choi, S. M. Disseler, D. A. Gilbert, G. Yin, Q. Shao, P. Deng, Y. Wu, X. Liu, X. Kou, S. Masashi, X. Han, C. Binek, S. Chambers, J. Xia, and K. L. Wang, *Advanced Materials* **32**, 2001460 (2020).
- [25] Y. Wu, W. Wang, L. Pan, and K. L. Wang, *Advanced Materials* **34**, 2105266 (2022).
- [26] S. Zhang, R. Wang, X. Wang, B. Wei, B. Chen, H. Wang, G. Shi, F. Wang, B. Jia, Y. Ouyang, F. Xie, F. Fei, M. Zhang, X. Wang, D. Wu, X. Wan, F. Song, H. Zhang, and B. Wang, *Nano Letters* **20**, 709 (2020).
- [27] W. H. Meiklejohn and C. P. Bean, *Physical Review* **102**, 1413 (1956).
- [28] J. Nogués and I. K. Schuller, *Journal of Magnetism and Magnetic Materials* **192**, 203 (1999).
- [29] M. Kiwi, *Journal of Magnetism and Magnetic Materials* **234**, 584 (2001).
- [30] R. Zhu, W. Zhang, W. Shen, P. K. J. Wong, Q. Wang, Q. Liang, Z. Tian, Y. Zhai, C.-w. Qiu, and A. T. S. Wee, *Nano Letters* **20**, 5030 (2020).
- [31] P. K. Manna and S. M. Yusuf, *Physics Reports* **535**, 61 (2014).
- [32] J. M. D. Coey, *Journal of Physics: Condensed Matter* **26**, 064211 (2014).
- [33] J. Nogués, C. Leighton, and I. K. Schuller, *Physical Review B* **61**, 1315 (2000).
- [34] H. K. Gweon, S. Y. Lee, H. Y. Kwon, J. Jeong, H. J. Chang, K.-W. Kim, Z. Q. Qiu, H. Ryu, C. Jang, and J. W. Choi, *Nano Letters* **21**, 1672 (2021).
- [35] G. Zheng, W.-Q. Xie, S. Albarakati, M. Algarni, C. Tan, Y. Wang, J. Peng, J. Partridge, L. Farrar, J. Yi, Y. Xiong, M. Tian, Y.-J. Zhao, and L. Wang, *Physical Review Letters* **125**, 047202 (2020).
- [36] V. Baltz, A. Manchon, M. Tsoi, T. Moriyama, T. Ono, and Y. Tserkovnyak, *Reviews of Modern Physics* **90**, 015005 (2018).

Figure captions

Figure 1. Negative exchange bias effect in $\text{CrI}_3/\text{MnBi}_2\text{Te}_4$ heterostructure device.

(a) The schematic device configuration. (b) The back-gate (V_{bg}) dependent longitudinal resistance (R_{xx}) of a $\text{CrI}_3/(5\text{-SLs})\text{MnBi}_2\text{Te}_4$ device (D1). Top inset is the optical image of D1 before the stacking of h-BN and graphite protective layers. Bottom inset is the atomic structure of MnBi_2Te_4 . Scale bar in the inset is $10 \mu\text{m}$. (c) The temperature dependent R_{xx} curve of D1 in field cooling processes. The dip or hump feature near 21 K indicates the Néel temperature of MnBi_2Te_4 thin flake. (d) Negative exchange bias effect and the training effect observed in D1.

Figure 2. Back-gate voltage (V_{bg}), cooling-field ($\mu_0 H_{\text{cf}}$) and temperature dependent exchange bias effect. (a, b) With a certain cooling-field (V_{bg}), the magnitude and sign of exchange bias effect measured under different V_{bg} (cooling-field) are almost unchanged in the $\text{CrI}_3/(5\text{-SLs})\text{MnBi}_2\text{Te}_4$ device (D1). (c) The exchange bias effect observed at different temperatures. With temperature increasing, the exchange bias disappears gradually. (d, e) Temperature dependent $\mu_0 H_{\text{eb}}$ (d) and $\mu_0 H_{\text{c}}$ (e) of different devices with different MnBi_2Te_4 thickness.

Figure 3. Positive exchange bias effect in partially covered $\text{CrI}_3/\text{MnBi}_2\text{Te}_4$ heterostructure devices. (a) The schematic device configuration. (b) The optical image of D4 before the stacking of h-BN and graphite protective layers. The scale bar is $10 \mu\text{m}$. (c, d) The temperature dependent evolution of positive exchange bias of D4 field cooled at 0.1 T (c) and -0.1 T (d). The V_{bg} is 0 V in these measurements. (e, f) The temperature dependent exchange bias field ($\mu_0 H_{\text{eb}}$) and coercive field ($\mu_0 H_{\text{c}}$) are

summarized and plotted. The $\mu_0 H_{eb}$ and $\mu_0 H_c$ are enhanced compared to D1 and D2 in Fig. 2. The partially covered device also shows a higher blocking temperature.

Figure 4. Negative and positive exchange bias effect with large $\mu_0 H_{eb}$ in CrI₃/MnBi₂Te₄ heterostructures. (a) The negative and positive exchange bias effect are observed in CrI₃/MnBi₂Te₄ heterostructures of different configurations, i.e., fully covered (left) and partially covered (right) configuration. These simplistic illustrations are ideal conjecture of spin textures of CrI₃/MnBi₂Te₄ heterostructures after field-cooling with a small cooling-field. In the fully (partially) covered device configuration, the spins of CrI₃ and MnBi₂Te₄ prefer a FM (AFM) coupling at the interface. (b) The $\mu_0 H_{eb}$ observed in this study and several other works are plotted. The solid symbols are TI related.

Figures

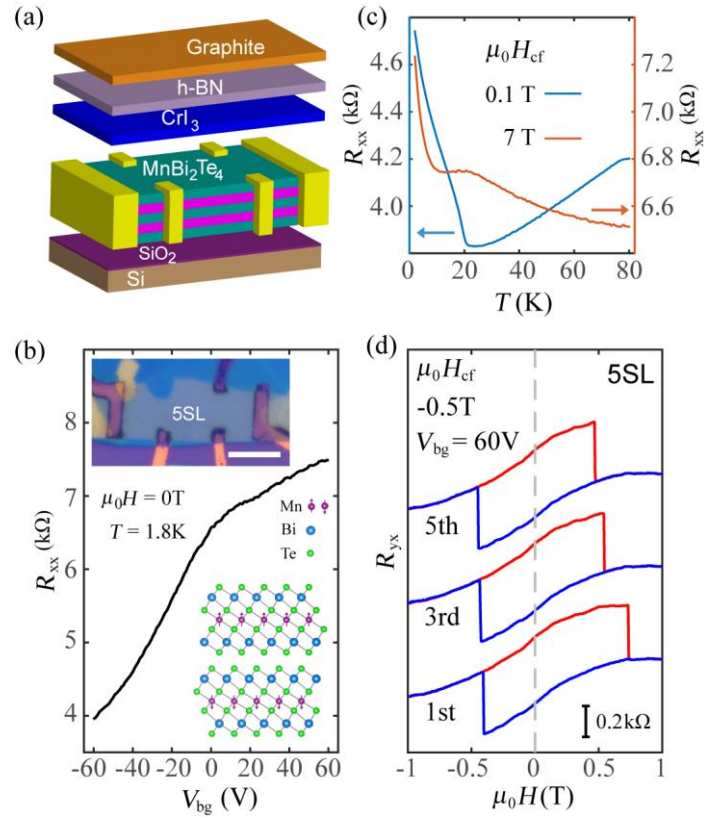


Figure 1. Ying et al

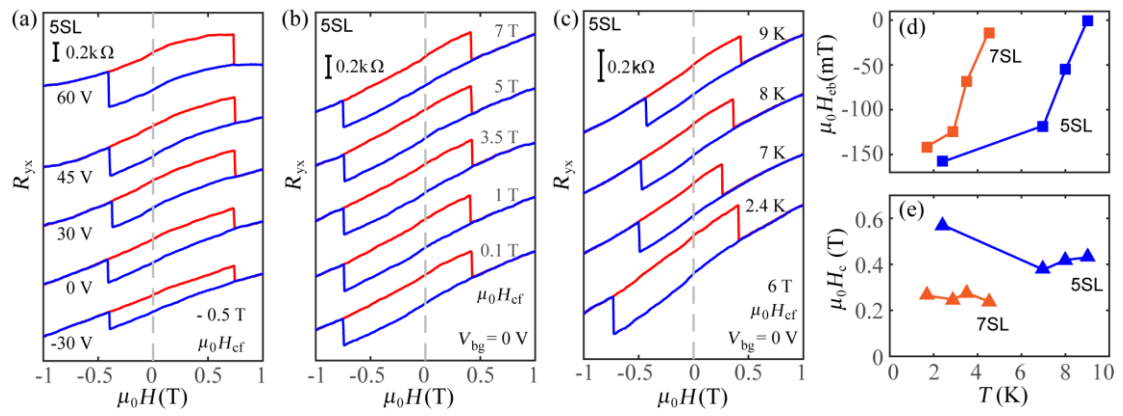


Figure 2. Ying et al

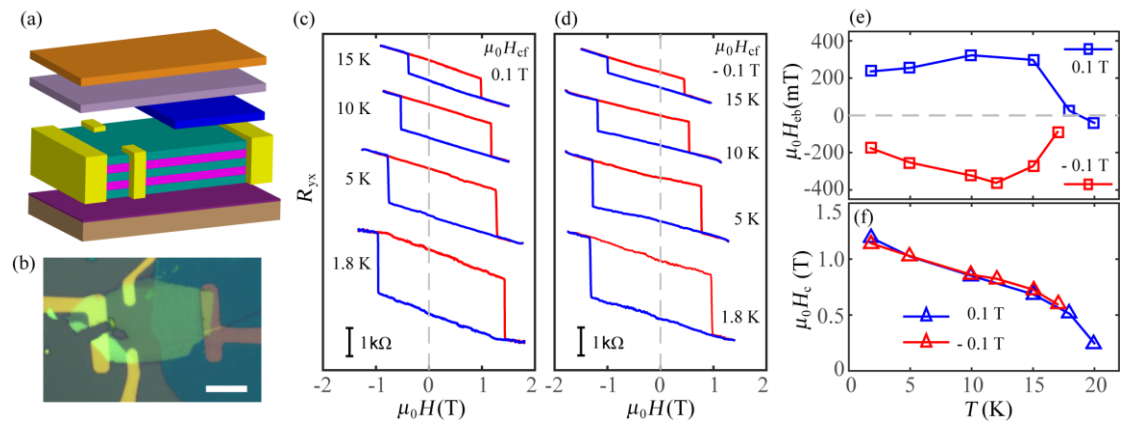


Figure 3. Ying et al

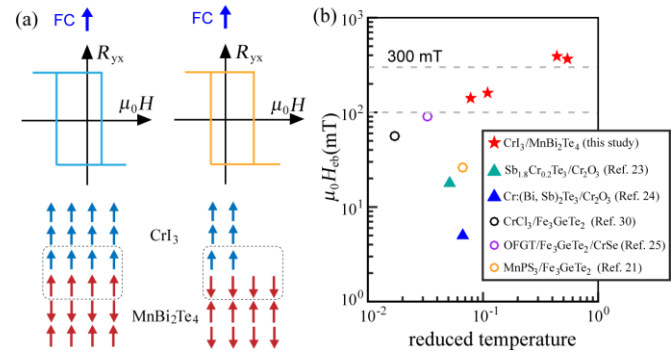


Figure 4. Ying et al